http://doi.org/10.29227/IM-2019-02-77 Submission date: 01-06-2019 | Review date: 07-06-2019

Use of Unmanned Aerial Vehicles for 3D topographic Mapping and Monitoring the Air Quality of Open-pit Mines

BUI Xuan Nam[1)], LEE Changwoo[2)], NGUYEN Quoc Long[1,*)], ADEEL Ahmad[3)], CAO Xuan Cuong[1)], NGUYEN Viet Nghia[1)], LE Van Canh[1)], NGUYEN Hoang[1)], LE Qui Thao[1)], DUONG Thuy Huong, NGUYEN Van Duc[2)]

[1)] Hanoi University of Mining and Geology, Vietnam
[2)] Dong-A University, Busan, Korea
[3)] University of the Punjab, Lahore, Pakistan

Corresponding author: nguyenquoclong@humg.edu.vn

Abstract. Recently remarkable advancement development of unmanned aerial vehicles (UAVs) has been observed and their applications have been shown in many fields such as agriculture, industry, and environmental management. However, in the mining industry, the application of UAV technology remains potential. This paper presents a low-cost unmanned aerial vehicle technology-based system for 3D mapping and air quality monitoring at open-pit mine sites in Vietnam. The system includes several dust sensors that are mounted on a low-cost rotary-wing type UAV. The system collects a variety of data, mainly images and airborne pollutant concentrations. To evaluate the performance of the proposed system, field tests were carried out at the Coc Sau coal mine. Based on the images transmitted to the ground monitoring station, large scale 3D topographic maps were successfully modeled. In addition, sensors mounted on the UAV system were able to monitor the levels of environmental variables associated with the air quality within the pit such as temperature, dust, CO, CO_2, and NOx. The field test results in this study illustrate the applicability of the low-cost UAV for the 3D mapping and the air quality monitoring at large and deep coal pits with relatively high accuracy.

1. Introduction

As one of the most important economic activities, the mining industry of Vietnam has been developing at a great pace. Coal produced by the Vietnam national coal-mineral industries holding corporation limited (Vinacomin) increased significantly from 27.5 million tons in 2004 to 47.5 million tons in 2010 (Tran & Nguyen, 2011). This accomplishment was attributed to the continuous application of advanced technologies in producing activities. In addition, Tran and Nguyen (2011) pointed out that it is necessary to continuously enhance the technology of all producing stages in order to achieve all

Vinacomin's goals. Mine surveying and environmental management are two of those important activities which have received great attention from both mining managers and scientists.

Traditional methods such as total station, the global navigation satellite system (GNSS) have been widely used in mining surveying with an accuracy of under 5 cm (Barry & Coakley, 2013). However, their main disadvantages are high cost and time consuming (Bui et al., 2016). In addition, the two methods meet many difficulties in areas with complicated terrains, especially unsafety for surveyors.

The mining industry of Vietnam has made a great contribution to the country's economy. However, this industry also inevitably leads to many environmental problems. In Vietnam, larger-scale open pit mines are often situated close proximity to population centers. For example, two of the largest open-pit coal mines in Vietnam, Coc Sau, and Deo Nai, are just about 1 km far from the Cam Pha city, Quang Ninh province (Figure 1). While blasting is an integral part of large-scale open-pit mining, it normally causes the emission of particulate material and gases potentially hazardous to health (Alvarado, Gonzalez, Fletcher, & Doshi, 2015). These activities generate particles and gases such as methane (CH_4), carbon dioxide (CO_2), nitrogen oxides (NO_x), and sulfur oxides (SO_x) that have potentially dangerous environmental and health impacts. It is noted that airblast, ground vibration, flyrock, toxic fumes, and particulate matter are the result of the blasting activity (Raj, 2005). All blasting events in mining areas emit the primary residue of Particulate matter, aerosols, ammonia, carbon dioxide (CO_2), nitrogen, nitrogen oxides (NO_x), and sulfur oxides (SO_x) (Alvarado et al., 2015). Although the exothermic reaction generates CO_2, water vapor, and Nitrogen (N_2) in a special case, other toxic fumes are proved to be produced in a range of concentrations as a result of environmental and technical factors (Attalla, Day, Lange, Lilley, & Morgan, 2007). In order to have proper management of air quality in mining areas, it is important to establish an effective monitoring system of air quality.

Recently, a rapid development in the unmanned aerial vehicle (UAV) technology has brought many benefits to not only military but also a wide range of civil fields such as logistics (Haidari et al., 2016; Olivares, Cordova, Sepúlveda, & Derpich, 2015), precise agriculture (Puri, Nayyar, & Raja, 2017; Rokhmana, 2015), forestry (Paneque-Gálvez, McCall, Napoletano, Wich, & Koh, 2014), urban management (Khan, Ectors, Bellemans, Janssens, & Wets, 2017; Salvo, Caruso, & Scordo, 2014; Spanogianopoulos, Zhang, & Spurgeon, 2017), hazardous and environmental management (Mourato, Fernandez, Pereira, & Moreira, 2017; Oleire-Oltmanns, Marzolff, Peter, & Ries, 2012), and mining industry. The preliminary successes of UAV applications have proved that this technology could be a promising technology and likely to be employed in a wider field. While the world has witnessed many excellent examples of using the UAV technology in the mining industry for topographical survey, safety investigation and other works (Sungjae Lee & Choi, 2016), this technology is still relatively new to Vietnam (Bui et al., 2016). For instance, the UAV technology was utilized to carry out a topographic survey of areas on the slope of an open-pit mine (McLeod et al., 2013). Another UAV based performance of topographic survey of an ore stockpile was given by Cryderman, Mah, and Shufletoski (2014). These authors used topographic data to estimate ore carrying capacity. S. Lee and Choi (2015) have proved that fixed-wing and rotary-wing UAVs, the most popular ones, can be used effectively in both small-scale and large-scale open-pit mines as a topographic surveying tool (S. Lee & Choi, 2015). For air quality monitoring in open-pit mine sites, results of the laboratory and field tests conducted by Alvarado et al., (2015) demonstrated the feasibility of coupling an opto-electronical dust sensor with UAVs.

As mentioned above, the application of UAVs has been proved as an alternative tool for both 3D mapping and the air quality monitoring. In this study, a low-cost UAV-based

system was employed to perform two-fold purposes at Coc Sau open-pit coal mine, one of the largest coal pit in Vietnam. This low-cost UAV system named as UMS-AM is designed to collect the varieties of data which can be used for optimizing mining operations and also control the atmospheric environment.

2. Description of the UMS-AM system

2.1 UAV platforms

The type of UAV is classified based on different but interrelated characteristics such as size and payload, wing types, flight endurance, flight range, altitude and capabilities (Berie & Burud, 2018). Based on wing types, there are two main types of UAV, namely the rotary-wing and fixed-wing UAVs. The latter is suitable for the applications that demand longer flight endurance, but large space is needed for take-off and landing. Although the former uses batteries and has shorter flight times (Paneque-Gálvez et al., 2014), it has been increasingly common because of its ability to take off and land vertically in the small space and to maintain position. Therefore, in this study, a rotary-wing UAV was considered as a feasible platform for the system. Specifically, its characteristics are in the following table 1.

Table 1. Specifications of major private UAV equipment

Name of UAV	Inspire 2
Weight	4000 g
Battery	4280 mAh
Camera	Multi: CMOS, 1" 20 MP
Max flight time	Approx. 27 min
Cruise speed	- P mode/A-mode: 16.4 ft/s (5 m/s) - S-mode: 19.7 ft/s (6 m/s)
Radio link range	7 km
Payload	Approx. 1.9 kg

The variety of UAV equipment allows users to have many different options. One of the major advantages of this UAV type is their low prices. However, the payload has to be taken into consi**d**eration as there are several air quality sensors and accessories mounted on the UAV. In this study, the DIJ Inspire 2 was utilized for the investigation as shown in figure 1.

Fig. 1. DJI Inspire 2 UAV (https://www.dji.com)

2.2 Sensors

2.2.1 Optical sensor (Inspire 2's camera parameters)

The Zenmuse X4S is a powerful camera featuring a 20 megapixel 1-inch sensor and a maximum ISO of 12,800. Dynamic range is increased from the Zenmuse X3 by 1 stop, with the signal to noise ratio and color sensitivity increased by 1.5 stops for next-level image quality. The Zenmuse X4S uses a DJI-designed compact lens with low dispersion and low distortion 24mm equivalent prime lens. This 84° FOV, high resolution lens makes the Zenmuse X4S as powerful during aerial imaging as it is on the ground. Combined with CineCore 2.0, the Inspire 2's powerful image processing system, it can record 4K/60 H.264 and 4K/30 H.265 videos at a 100Mbps bitrate, and oversample 5.2K video into 4K video in real-time, capturing fine image details. In Burst Mode, the Zenmuse X4S supports 14fps shooting at 20 megapixels in both JPEG and DNG formats. It is able to make the difficult balance between agility and image quality (https://www.dji.com/zenmuse-x4s).

2.2.2 Air quality monitoring system

To evaluate mine pit the air quality within the atmosphere of a deep pit mine, the levels of four major pollutants including PM_{10}, CO, NO, and NO_2 were measured by UAV. Several sensors described in Table 2 were attached to UAV for monitoring. Due to the load limitation of UAV, light and compact sensors were packed in a perforated box and mounted on the vehicle. Figure 3 shows the monitoring box installation and a picture of UAV flight.

The communication link played an important role between the data collection and transmission. The data transmission should satisfy the requirements of stability and reliability when the UAV equipped with the monitoring sensor box reach high altitude. Thus, a smartphone or a tablet was attached into the monitoring box as a relay station and also transceiver to store the measurement data. The structure of the UAV air quality monitoring platform and the system concept are illustrated in Figure 2. In this study, prior to flying the UAV, all the sensors were calibrated.

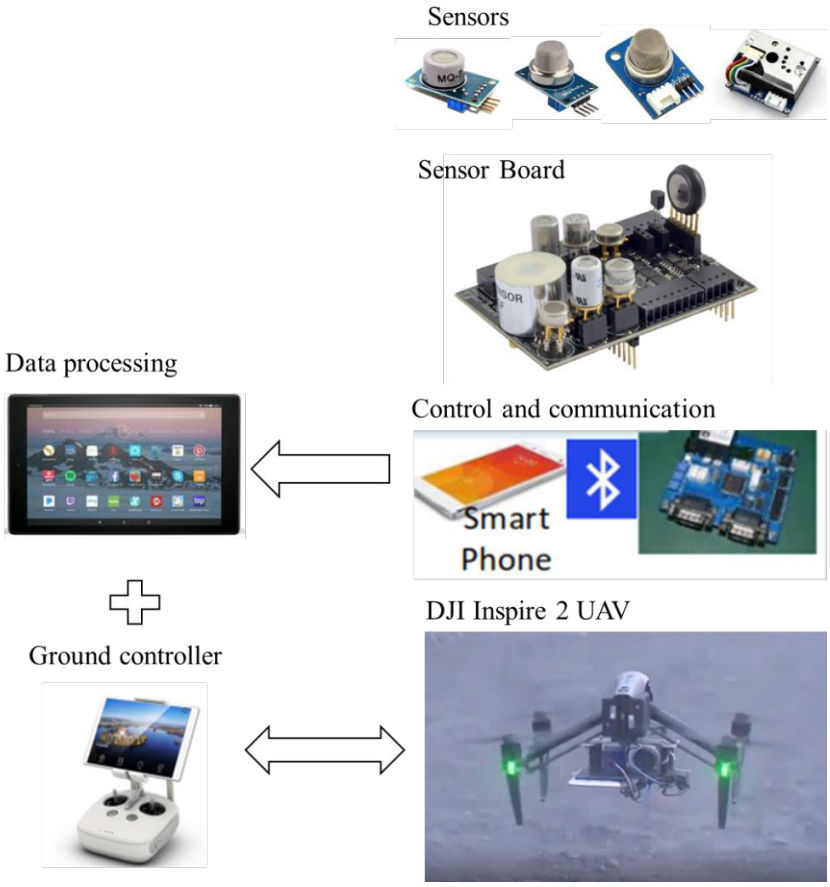

Fig. 2. Structure of the UAV air quality monitoring platform and system concept for collecting a drone mounted air quality sensor

In addition, two ground monitoring stations were installed on the top of the pit mainly to monitor the atmospheric condition of the free stream including the barometric pressure, temperature and wind velocity along with the direction.

Table 2. Specifications of the air quality monitoring sensors

Monitoring Target	Sensor category	Range	Precision	Resolution
PM_{10}	Laser dust sensor	0-500 µg/m^3	± 10%	0.3 µg/m3
CO	Electrochemistry sensor	0-750ppm	± 5% ppm	1 ppm
NO	Electrochemistry sensor	0-250ppm	± 5% ppm	1 ppm
NO_2	Electrochemistry sensor	0-20ppm	± 5% ppm	0.1 ppm

Fig. 3. Air quality monitoring components of the UMS-AS system

3. Study site

Coc Sau, as shown in Figure 4, was the second largest and the deepest open-pit mine in Vietnam at the time of the study. Coal produced at the Coc Sau mine contributed over 2 million tons to the VINACOMIN's production.

4. Operation and data processing

4.1 3D mapping section

Flight plans for aerial photography are established using the Pix4DCapture software installing in an Ipad tablet. Considering the maximum flight time during battery charge, one of the flight routes is shown in Fig 5a, and the flight altitude is calculated by considering the topographic altitude of the surrounding areas. In addition, the lateral vertical overlaps of the aerial photographs to be photographed were set to 80%.

In order to improve the accuracy of terrain survey results using UAVs, it is necessary to correct the data using ground control points. In this study, 35 GCPs were installed in the study area using markers (Fig 5b). We used GNSS CORs to measure the coordinates of these GCPs. We measured the X, Y and Z coordinates of the GCPs by receiving the satellite signals for about one minute after vertically positioning the CORs rover at the center of the markers.

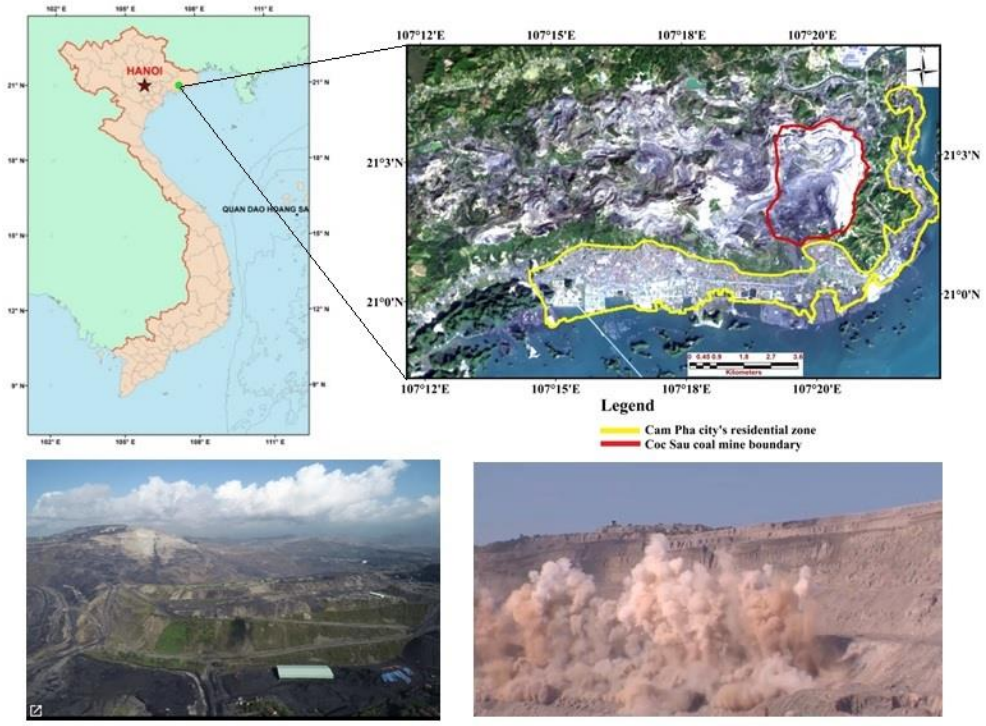

Fig. 4. Location of the study area in Cam Pha city, Quang Ninh province, Vietnam

There is a variety of software for processing aerial photographs such as Pix4D, Autodesk 123D Catch, DroneMapper, Acute3D, TBC, Agisoft Photoscan, and PhotoModeler. However, Agisoft Photoscan has been approved to be the best one (Sona, Pinto, Pagliari, Passoni, & Gini, 2014). Therefore, in this study, Agisoft Photoscan (ver 1.3.1) was used to process aerial photographs captured at the site (Fig 5d). When these photos are entered into Agisoft Photoscan, key points that can be identified simultaneously from multiple images are automatically extracted. With GNSS GCPs, 3D point clouds are built for automatic photo matching process. In the next stage, the automatic aerial triangulation (AAT) procedure is undertaken including the three following steps: (i) calculate both external and internal orientation parameters; (ii) perform the least squares block adjustment; and (iii) build mesh, digital surface model, and orthophoto.

4.2 Air quality monitoring measurement

This study had two-fold purposes for monitoring the atmospheric environment and understanding the pollutants dispersion mechanism. Investigation of the air quality was carried out within a large and deep pit mine. Pollutants dispersion in a deep pit depends on the surface wind and the air density differences between the in and outside of the pit.

However, it is well known that strong nocturnal inversions occur in valleys and mountain basins on calm, clear night (e.g. Hibberd 2003, Clements et al 2003) but there was almost no data related to the existence of the inversion layer at the deep pits. Thus, this

study measured vertical temperature profiles to identify the temperature gradient to determine the airflow stability during the study.

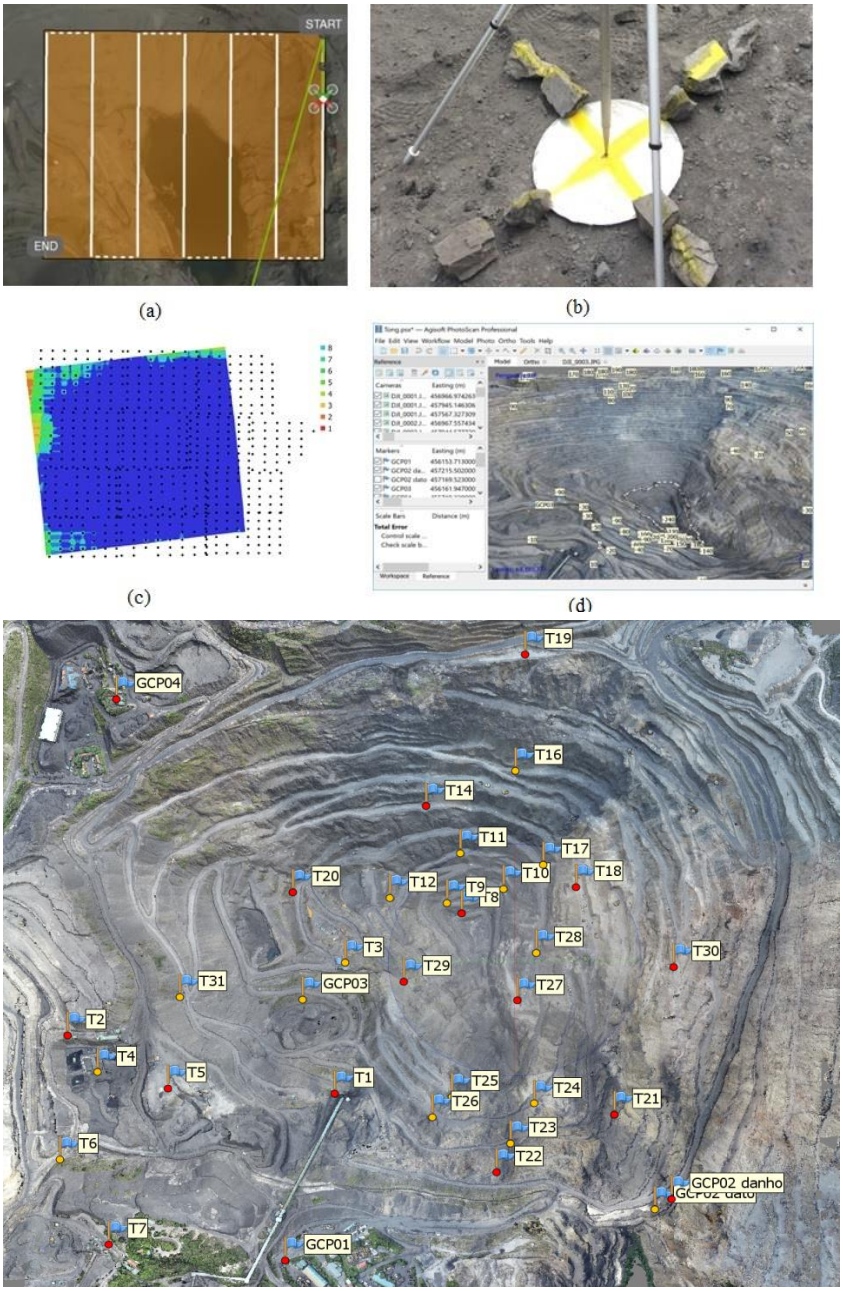

Fig. 5. 3D mapping steps in Coc Sau coal mine (a) Flight route and shooting points designed for the study area; (b) The designed marker and Ground control points (GCPs) measured by GNSS CORs; (c) Camera locations and image overlap; (d) Processing UAV photos with Agisoft Photoscan software; (f) distribution of calibrated and checked points

Due to the limited battery capacity of UAV, the UAV has less hover time with more load. The total load including sensors and other accessories was 1.0 kg, the hover time was about 25 minutes. However, by excluding the time for starting and landing, it was necessary to shorten the hover time to 15 minutes. Figure 6 shows the UAV flight paths to measure the atmospheric environment problems within the pit. The space within the pit was divided into two sections; H1 at -140m and H2 at 120m as shown in Figure 6. UAV flew through these zones in a systematical way. The data collected were utilized to make 3D environment maps.

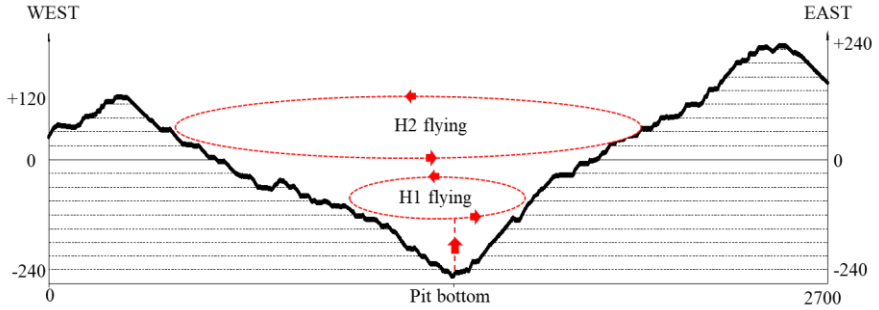

Fig. 6. UAV flight paths to measure the atmospheric environment at pit

For the second purpose to measure the vertical temperature profiles within the pit, the UAV was flown along the flight paths shown in Figure 7. UAV started at the center of the pit bottom and flew along the vertical line to 250m above the sea level. The flight was made twice a day, before the sunrise and after the sunset.

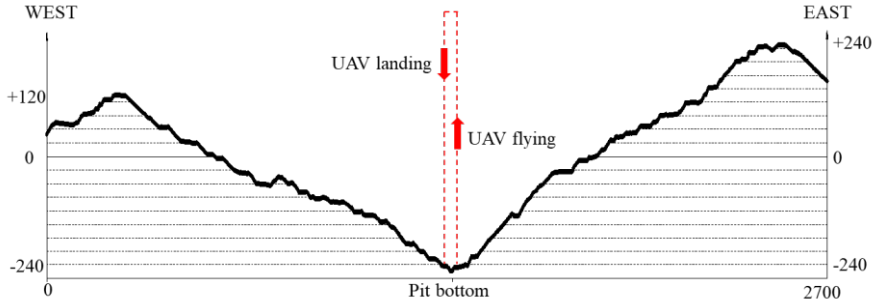

Fig. 7. UAV flight to measure the vertical temperature profiles

4.3 Accuracy assessment of the digital surface model

Accuracy assessment of the Digital Surface Model (DSM) is an important task, and without this task, the DSM is useless. In this project, both the horizontal and vertical assessments were carried out by comparing DSM with the GCPs measured by a Leica total station in term of Root Mean Square Error (RMSE). More specifically, assessments in easting ($RMSE_X$), northing ($RMSE_Y$), vertical ($RMSE_Z$), and all components ($RMSE_{XYZ}$)

were used, as suggested in Agüera-Vega (Agüera-Vega, Carvajal-Ramírez, & Martínez-Carricondo, 2016), using equations as follows:

$$\Delta X = \mathrm{X_{DSM}} - \mathrm{X_{GCP}} \tag{1}$$

$$\Delta Y = \mathrm{Y_{DSM}} - \mathrm{Y_{GCP}} \tag{2}$$

$$\Delta Z = \mathrm{Z_{DSM}} - \mathrm{Z_{GCP}} \tag{3}$$

$$\Delta XYZ = \mathrm{XYZ_{DSM}} - \mathrm{XYZ_{GCP}} \tag{4}$$

$$RMSE_{\mathrm{X}} = \mathrm{SQRT}\left[(1/n) \sum_{i=1}^{n} (\mathrm{X_{DSM}} - \mathrm{X_{GCPi}})^2 \right] \tag{5}$$

$$RMSE_{\mathrm{Y}} = \mathrm{SQRT}\left[(1/n) \sum_{i=1}^{n} (\mathrm{Y_{DSM}} - \mathrm{Y_{GCPi}})^2 \right] \tag{6}$$

$$RMSE_{\mathrm{Z}} = \mathrm{SQRT}\left[(1/n) \sum_{i=1}^{n} (\mathrm{Z_{DSM}} - \mathrm{Z_{GCPi}})^2 \right] \tag{7}$$

$$RMSE_{\mathrm{XYZ}} = \mathrm{SQRT}\left[(1/n) \sum_{i=1}^{n} ((X_{\mathrm{DSM}} - X_{\mathrm{GCPi}})^2 + (Y_{\mathrm{DSM}} - Y_{\mathrm{GCPi}})^2 + (Z_{\mathrm{DSM}} - Z_{\mathrm{GCPi}})^2) \right] \tag{8}$$

where $\mathrm{X_{GCPi}}$ and $\mathrm{X_{DSM}}$ are the X-coordinate component of GCP and corresponding coordinate in DSM, respectively; $\mathrm{Y_{GCPi}}$ and $\mathrm{Y_{DSM}}$ are the Y-coordinate component of GCP and corresponding coordinate in DSM, respectively; $\mathrm{Z_{GCPi}}$ and $\mathrm{Z_{DSM}}$ are the Z-coordinate component of GCP and corresponding coordinate in DSM, respectively.

5. Some of the field test results

5.1 3D mapping

Table 3 shows the aerial photographs of the study area using our designed system. 687 aerial photographs were shot according to the flight plan (Fig 5c). However, for the area where air quality was monitored, there were 56 photos. The average spatial resolution of the aerial photographs was about 8.55 cm/pixel. It took about 6 hours to process 687 aerial images using Agisoft Photoscan.

Table 3. Data acquisition

Number of images	687	Camera stations	680
Flying attitude	327 m	Tie points	527,464
Ground resolution	8.55 cm/pixel	Projections	2280976

To determine the best camera-lens parameters in this research, an optimization process was carried out. For this task, the 35 GCPs were split into two subsets: (i) the first one is a calibrating dataset that accounts for 17 GCPs of the total GCPs and was used for the calibration of the camera-lens model and the bundle adjustment; (ii) the second one is a checking dataset that consists of the remaining GCPs. 18 GCPs were used for checking the final model and confirming its accuracy. Distribution of these GCPs in this study area is

shown in Fig. 5e. This is because these were unsafe areas to reach due to the coal seams still were exploiting.

After the following steps: photo align, camera calibration, bundle adjustment, cloud point building, and mesh creation, the digital surface model of the mine was produced (Fig. 8c). For the model calibration, RMSE for X, Y, Z, XYZ is 1.1 cm, 1.7 cm, 4.9 cm, and 5.1 cm, respectively. The largest error for X is 2.0 cm and for Y is 5.4 cm whereas the largest error for Z is 9.5 cm. The largest error for XYZ is 9.5 cm (Table 4). These indicate that the close fit of the DSM model with the calibrating dataset.

Table 4. RMSE in X, Y, Z, XY and XYZ of GCPs used for the model calibration.

Calibration Points	ΔX (m)	ΔY (m)	ΔXY (m)	ΔZ (m)	Δ XYZ (m)
GCP01	0.003	0.002	0.004	0.011	0.012
GCP02 danho	-0.004	-0.014	0.015	-0.02	0.058
GCP04	-0.012	0.001	0.012	0.021	0.016
T2	-0.004	0.013	0.014	0.013	0.019
T5	0.007	0.007	0.010	-0.016	0.019
T7	0.005	-0.002	0.005	-0.054	0.054
T8	-0.02	-0.028	0.034	-0.063	0.072
T14	0.015	-0.012	0.019	-0.054	0.057
T18	0.004	-0.007	0.008	-0.025	0.026
T19	-0.008	0.001	0.008	0.095	0.095
T20	-0.007	-0.003	0.008	-0.014	0.016
T21	-0.007	-0.011	0.013	0.091	0.092
T22	0.006	-0.008	0.010	0.004	0.011
T27	-0.025	-0.017	0.030	0.063	0.07
T29	-0.016	0.012	0.020	0.079	0.081
T30	-0.007	-0.013	0.015	-0.028	0.032
T1	-0.004	-0.008	0.009	-0.017	0.019
Total	0.011	0.017	0.016	0.049	0.051

Table 5. RMSE in X, Y, Z, and XYZ of check points in this project.

Check points	ΔX (m)	ΔY (m)	ΔXY (m)	ΔZ (m)	Δ XYZ (m)
GCP03	0.120	0.166	0.205	-0.195	0.283
T3	-0.060	-0.020	0.063	-0.080	0.102
T4	-0.098	0.000	0.098	0.128	0.161
T6	-0.005	-0.032	0.032	-0.207	0.210
T9	0.053	-0.003	0.053	-0.204	0.309
T10	0.069	0.037	0.078	0.255	0.267

T11	0.094	-0.094	0.133	0.148	0.199
T12	0.022	0.003	0.022	-0.148	0.150
T15	0.035	-0.011	0.037	0.090	0.097
T16	0.044	-0.032	0.054	-0.035	0.065
T17	0.033	-0.089	0.095	-0.081	0.125
T23	-0.016	-0.064	0.066	-0.075	0.068
T24	0.006	-0.058	0.058	-0.071	0.059
T25	0.070	0.077	0.136	0.085	0.144
T26	-0.079	0.002	0.079	-0.071	0.079
T28	-0.108	-0.017	0.169	0.159	0.232
T31	0.082	-0.062	0.128	0.068	0.145
GCP02 dato	0.006	0.015	0.016	0.138	0.139
Total	0.066	0.061	0.090	0.138	0.164

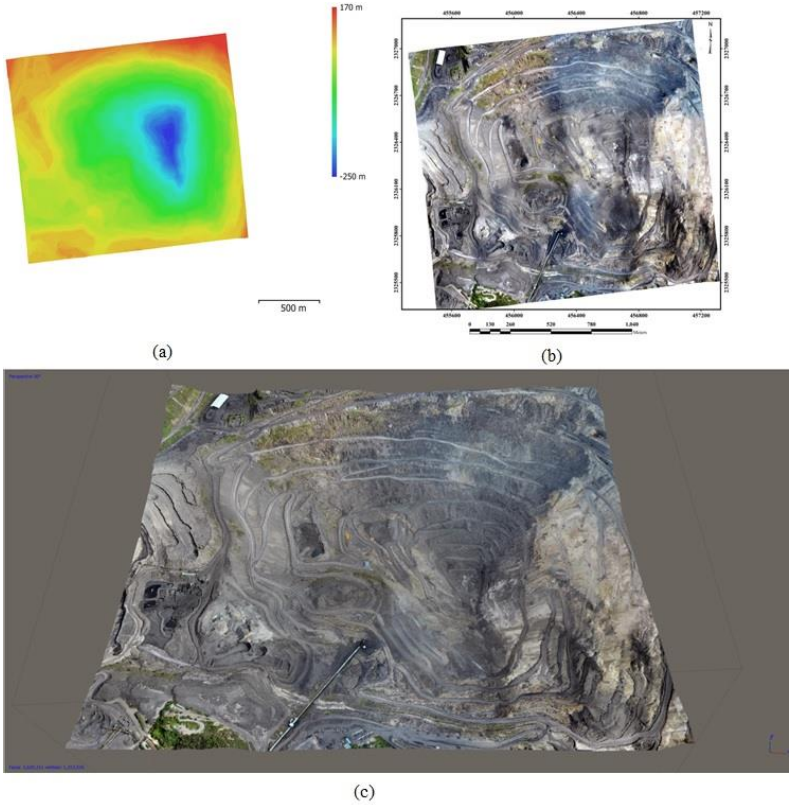

Fig. 8. Results of 3D mapping using the UMS-AM system (a) Digital Elevation Model (DEM); (b) Othorphoto; (c) The 3D model of the Coc Sau coal mine.

Fig. 8a shows the DEM and orthoimage produced using the proposed system with a resolution of 34 cm/pixel and 8.5 cm/pixel, respectively. In addition, Fig. 8c shows the topographical results of the study area in three dimensions. For the accuracy assessment of the results, the root mean square error (RMSE) for the position coordinates of the GCPs in the X, Y, and Z directions is used.

Since the calibrating dataset was used for both the optimization process and the goodness-of-fit, the result may be too positive. Therefore, the checking dataset that was not used in the calibration phase was used to assess the accuracy of the DSM model. The result is shown in Table 5. It could be seen that the RMSE of X, Y, Z, XYZ are 6.6 cm, 6.1 cm, 13.8 cm, and 16.4 cm, respectively. The highest error for X is 12.0 cm and for Y is 16.6 cm whereas the highest error for Z is 25.5 cm and the highest error for XYZ is 28.3 cm (Table 5). These indicate that the accuracy of the DSM model is appropriate with the accuracy requirement for mine surveying missions.

5.2 Air monitoring

Figure 9 shows the environment maps plotted in terms of CO, Dust (PM_{10}), NO and temperature. These maps were generated by ArcGIS (version 10.2). In addition, in order to complete the 3D contours, the Inverse Distance Weighted (IDW) interpolation method was employed. These maps show the environmental pollution profiles at the altitude of +120m.

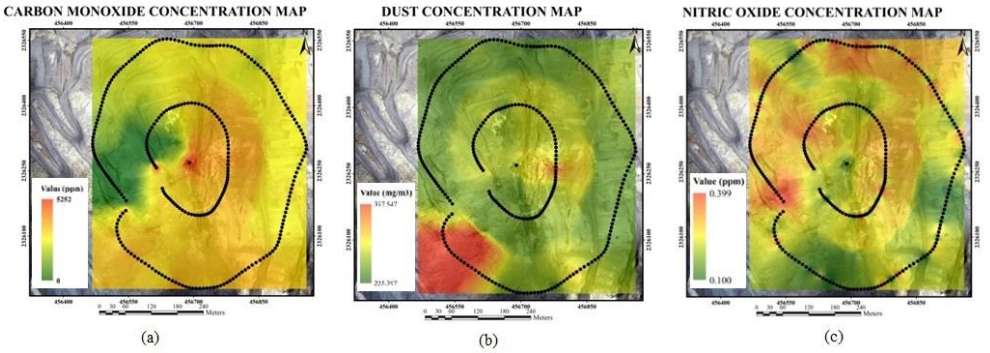

Fig. 9. Concentration maps of air components (a) CO; (b) Dust (PM10); (c) NO

The dispersion mechanism within a deep open pit mine is complicated due to the effect of topographic, thermal and meteorological factors. The meteorological conditions within the deep open pit coal mine are significantly affected by temperature (stability) and roughness conditions which ultimately generate complex dispersion phenomenon including separation of the atmospheric boundary layer, recirculation, re-suspension, and settling of PM_{10} (Bitkolov, 1969; Grainger & Meroney, 1993). Based on the site measurement, Figure 10 shows the vertical temperature profiles.

The possible temperature inversion effect was observed in Figure 10 (a) which was based on the the first day measurement before the sunrise. However, this phenomenon was not detected clearly in the other days. Further, the dispersion of air pollutants is dependent on the Pasquill stability of the atmosphere classes in Table 6.

Table 6. Pasquill stability classes by the vertical temperature gradient

Stability class	Vertical temp gradient, ΔT/ΔZ (DegC/100m)	Definition
A	-1.9	very unstable
B	-1.9 to -1.7	unstable
C	-1.7 to -1.5	slightly unstable
D	-1.5 to -0.5	neutral
E	-0.5 to 1.5	slightly unstable
F	1.5 to 4.0	stable
G	> 4.0	very stable

Table 7 shows the vertical temperature gradients for three days' experiments. The temperature gradient was in the range of 0.64-1.53 ^{o}C/100 m and the atmosphere can be classified as E and F. This implies "slightly unstable" and "stable" which indicate the dispersion of pollutants generated within the pit is hardly dispersed out of the deep pit. This resulted in high dust concentrations observed during the study in Figure 9 (b).

Table 7. Vertical temperature gradients during the study

Category	Before sunrise		After sunset	
	Upward flight	Downward flight	Upward flight	Downward flight
1st day measurement	1.17	1.53	0.64	0.68
2nd day measurement	0.68	0.84	1.53	1.28
3rd day measurement	1.21	1.12	1.13	1.23

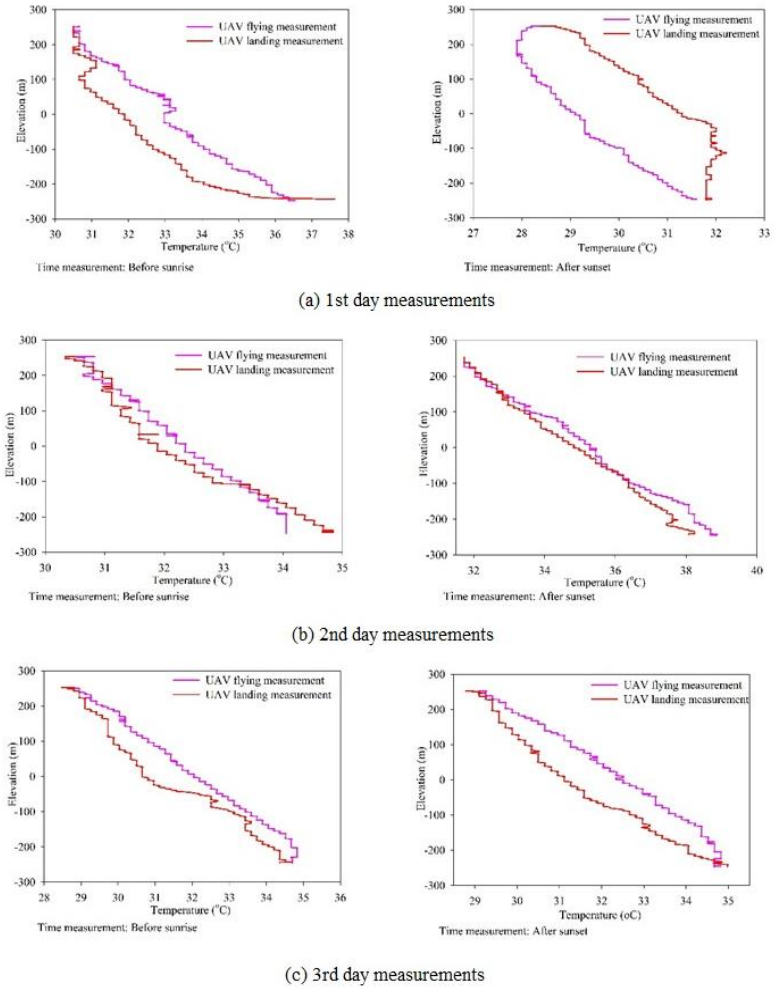

Fig. 10. Vertical temperature profiles by UAV measurement

6. Conclusion

In this study, a UAV-based system has been developed ultimately for the topographical survey and the air quality management in the mining industry. The UAV system includes a DJI Inspire 2 equipped by the RGB Zenmuse X4S camera, air quality monitoring sensors and data logging system. Through the site study, the system proved to be a safe, effective and economical tool for environmental management. Some of the limitations experienced during the study were closely related to the UAV system itself; the limitation on UAV allowable load was the most significant problem for the monitoring purposes. One of the advantages of the low-cost UAV system is that 3D models can be generated easily without additional efforts, while the system equipped with low-cost reliable sensors clearly show the applicability of the mine environment monitoring system within the large and deep pit mines.

For the accuracy of 3D models, the result showed that the DSM model has high accuracy; RMSE in the calibrating dataset is 2 cm and 4.9 cm for vertical and horizontal, respectively indicating high success-rate of fit, whereas RMSE in the checking dataset is 13.8 cm and 9 cm for vertical and horizontal, indicating high accuracy. These indicate that the processes of capturing images, establishment of GCPs, and photogrammetric processing were carried out successfully.

Ultimately, pollutant control measures can be derived by the system, since the air pollution profiles are visible in the 3D maps and the main causes of the pollution can be easily verified based on the 3D maps.

7. Acknowledgements

Paper was presented during the 5th POL – VIET International Conference Scientific-Research Cooperation between Vietnam and Poland, 08-10.07.2019, AGH UST, Krakow, Poland. This research was supported by the Ministry of Education and Training of Vietnam (MOET) under grant number B2018-MDA-03SP and by the Research Institute for Mining Electro-Mechanics of Hanoi University of Mining and Geology.

8. References

1. Agüera-Vega, F., Carvajal-Ramírez, F., & Martínez-Carricondo, P. (2016). Accuracy of Digital Surface Models and Orthophotos Derived from Unmanned Aerial Vehicle Photogrammetry. *Journal of Surveying Engineering*, 04016025.
2. Alvarado, M., Gonzalez, F., Fletcher, A., & Doshi, A. (2015). Towards the Development of a Low Cost Airborne Sensing System to Monitor Dust Particles after Blasting at Open-Pit Mine Sites. *Sensors, 15*(8), 19667. Retrieved from http://www.mdpi.com/1424-8220/15/8/19667
3. Attalla, M., Day, S., Lange, T., Lilley, W., & Morgan, S. (2007). *NOx Emissions from Blasting in Open Cut Coal Mining in the Hunter Valley*. Retrieved from ACARP: Newcastle, Australia,:
4. Barry, P., & Coakley, R. (2013). Accuracy of UAV photogrammetry compared with network RTK GPS. *Int. Arch. Photogramm. Remote Sens, XL-1 W*, 27-31.
5. Berie, H. T., & Burud, I. (2018). Application of unmanned aerial vehicles in earth resources monitoring: focus on evaluating potentials for forest monitoring in Ethiopia. *European Journal of Remote Sensing, 51*(1), 326-335. doi:10.1080/22797254.2018.1432993
6. Bitkolov, N. Z. (1969). Wind and Temperature of quarry atmospheres. *Fiziko-Tekhnicheskie Problemy Razrabotki Poleznykh Iskopaemykh*(5), 66-73.
7. Bui, T. D., Nguyen, C. V., Hoang, M. H., Dong, B. P., Nhu, V. H., Tran, T. A., & Nguyen, Q. M. (2016). *Xây dựng mô hình số bề mặt và bản đồ trực ảnh sử dụng công nghệ đo ảnh máy bay không người lái.* Paper presented at the Hội nghị khoa học: Đo đạc bản đồ với ứng phó biến đổi khí hậu, Hà Nội.
8. Cryderman, C., Mah, S. B., & Shufletoski, A. (2014). Evaluation of UAV Photogrammetric Accuracy for Mapping and Earthworks Computations. *GEOMATICA, 68*(4), 309-317. doi:10.5623/cig2014-405
9. Grainger, C., & Meroney, R. N. (1993). *Boundary-Layer Meteorol*: Kluwer Academic Publishers.
10. Haidari, L. A., Brown, S. T., Ferguson, M., Bancroft, E., Spiker, M., Wilcox, A., . . . Lee, B. Y. (2016). The economic and operational value of using drones to

transport vaccines. *Vaccine, 34*(34), 4062-4067. doi:10.1016/j.vaccine.2016.06.022
11. Khan, M. A., Ectors, W., Bellemans, T., Janssens, D., & Wets, G. (2017). UAV-Based Traffic Analysis: A Universal Guiding Framework Based on Literature Survey. *Transportation Research Procedia, 22*, 541-550. doi:https://doi.org/10.1016/j.trpro.2017.03.043
12. Lee, S., & Choi, Y. (2015). On-site demonstration of topographic surveying techniques at open-pit mines using a fixed-wing unmanned aerial vehicle (drone). *Tunnel & Underground Space, 25*, 527–533.
13. Lee, S., & Choi, Y. (2016). Reviews of unmanned aerial vehicle (drone) technology trends and its applications in the mining industry. *Geosystem Engineering, 19*(4), 197-204. doi:10.1080/12269328.2016.1162115
14. McLeod, T., Samson, C., Labrie, M., Shehata, K., Mah, J., Lai, P., . . . Elder, J. H. (2013). Using Video Acquired from an Unmanned Aerial Vehicle (UAV) to Measure Fracture Orientation in an Open-Pit Mine. *GEOMATICA, 67*(3), 173-180. doi:10.5623/cig2013-036
15. Mourato, S., Fernandez, P., Pereira, L., & Moreira, M. (2017). *Improving a DSM Obtained by Unmanned Aerial Vehicles for Flood Modelling*. Paper presented at the IOP Conf. Series: Earth and Environmental Science.
16. Oleire-Oltmanns, S., Marzolff, I., Peter, K., & Ries, J. (2012). Unmanned Aerial Vehicle (UAV) for Monitoring Soil Erosion in Morocco. *Remote Sens., 4*(11), 3390-3416. doi:10.3390/rs4113390
17. Olivares, V., Cordova, F., Sepúlveda, J. M., & Derpich, I. (2015). Modeling Internal Logistics by Using Drones on the Stage of Assembly of Products. *Procedia Computer Science, 55*, 1240-1249. doi:https://doi.org/10.1016/j.procs.2015.07.132
18. Paneque-Gálvez, J., McCall, M. K., Napoletano, B. M., Wich, S. A., & Koh, L. P. (2014). Small drones for community-based forest monitoring: An assessment of their feasibility and potential in tropical areas. *Forests, 5(6)*, 1481–1507.
19. Puri, V., Nayyar, A., & Raja, L. (2017). Agriculture drones: A modern breakthrough in precision agriculture. *Journal of Statistics and Management Systems, 20*(4), 507-518. doi:10.1080/09720510.2017.1395171
20. Raj, R. (2005). *Sustainable mining systems and technologies in Sustainable Mining Practices*. USA: Taylor & Francis: Oak Brook.
21. Rokhmana, C. A. (2015). The Potential of UAV-based Remote Sensing for Supporting Precision Agriculture in Indonesia. *Procedia Environmental Sciences, 24*(Supplement C), 245-253. doi:https://doi.org/10.1016/j.proenv.2015.03.032
22. Salvo, G., Caruso, L., & Scordo, A. (2014). Urban Traffic Analysis through an UAV. *Procedia - Social and Behavioral Sciences, 111*, 1083-1091. doi:https://doi.org/10.1016/j.sbspro.2014.01.143
23. Sona, G., Pinto, L., Pagliari, D., Passoni, D., & Gini, R. (2014). Experimental analysis of different software packages for orientation and digital surface modelling from UAV images. *Earth Science Informatics, 7*(2), 97-107. doi:10.1007/s12145-013-0142-2
24. Spanogianopoulos, S., Zhang, Q., & Spurgeon, S. (2017). Fast Formation of Swarm of UAVs in Congested Urban Environment. *IFAC-PapersOnLine, 50*(1), 8031-8036. doi:https://doi.org/10.1016/j.ifacol.2017.08.1228
25. Tran, X. H., & Nguyen, A. T. (2011). *Đổi mới, hiện đại hóa, khai thác và tuyển, chế biến nhằm phát triển bền vững ngành than - khoáng sản.* Paper presented at the Hội nghị khoa học kỹ thuật mỏ toàn quốc - 2011, Nha Trang.